IOPscience iopscience.iop.org

Home Search Collections Journals About Contact us My IOPscience

Spatially and temporally resolved near-field spectroscopy of single GaAs quantum wires

This article has been downloaded from IOPscience. Please scroll down to see the full text article.

1999 J. Phys.: Condens. Matter 11 5889

(http://iopscience.iop.org/0953-8984/11/31/301)

View the table of contents for this issue, or go to the journal homepage for more

Download details:
IP Address: 171.66.16.214
The article was downloaded on 15/05/2010 at 12:18

Please note that terms and conditions apply.

J. Phys.: Condens. Matter **11** (1999) 5889–5900. Printed in the UK PII: S0953-8984(99)01385-5

Spatially and temporally resolved near-field spectroscopy of single GaAs quantum wires

V Emiliani, T Günther, F Intonti, A Richter, C Lienau and T Elsaesser
Max-Born-Institut für Nichtlineare Optik und Kurzzeitspektroskopie, D-12489 Berlin, Germany

Received 28 January 1999, in final form 30 April 1999

Abstract. Single GaAs quantum wires grown on patterned (311)A GaAs substrates are studied by steady-state and time-resolved near-field optical spectroscopy with a spatial resolution of 250 nm. The photoluminescence and photoluminescence excitation spectra as well as lateral variations of the quasi-one-dimensional confinement potential of the quantum wire are determined by measurements in the temperature range from 10 to 300 K. Diffusive transport of excitons and trapping into the quantum wire are directly monitored in picosecond luminescence experiments, allowing a quantitative measurement of exciton mobility. First near-field pump–probe experiments with femtosecond time resolution demonstrate the potential of this technique for monitoring spatio-temporal dynamics on ultrafast time scales.

1. Introduction

The electronic and optical properties of quantum confined systems have received substantial interest and semiconductor nanostructures represent an important class of model systems for studying fundamental physics on a nanometre scale and for device applications. Both the dimensionality and the geometrical dimensions of semiconductor nanostructures can be varied in a controlled way using epitaxial techniques of crystal growth. The recent progress of such techniques has allowed for realizing quasi-one-dimensional nanostructures, i.e. quantum wires, of high structural quality. Individual quantum wires and arrays of coupled quantum wires have been produced by growth on tilted or prestructured substrates or by cleaved-edge overgrowth of quantum wells [1–3].

Analysing low-dimensional confinement potentials which are related to local variations of the electronic bandstructure, and processes of carrier transport and trapping in real space, requires experimental probes providing nanometre spatial resolution. For optical measurements, this demand is difficult to fulfil as the fundamental resolution limit of classical microscopy is set by the optical wavelength which is typically on the order of 1 μm. The resolution limit is overcome by near-field scanning optical microscopy (NSOM) where the sample is put into the near field of an aperture of sub-wavelength diameter [4, 5]. In the near-field region below the aperture, the resolution is determined by the diameter of the aperture and values down to approximately 50 nm have been reported. Techniques of time-resolved optical spectroscopy can be combined with NSOM and—thus—high spatial and temporal resolution can be achieved [6–8]. In this paper, we present a near-field optical study of single GaAs quantum wires. Steady-state near-field spectroscopy is applied to analyse the quasi-one-dimensional subband structure and the lateral confinement potential. Processes of exciton transport and carrier trapping are studied in picosecond NSOM experiments, allowing

0953-8984/99/315889+12$30.00 © 1999 IOP Publishing Ltd

a quantitative measurement of exciton mobilities. In the final part of the paper, we discuss first near-field pump–probe experiments with a time resolution of about 200 fs.

2. Experimental techniques

Figure 1 shows a schematic of the quantum wire structure investigated in our experiments. The sample was grown by molecular beam epitaxy on patterned GaAs(311)A substrates [9]. Patterning creates 15 to 20 nm high sidewalls of mesa stripes along the $[01-1]$ direction. On this substrate, a nominally 6 nm thick GaAs quantum well layer clad between 50 nm thick $Al_{0.5}Ga_{0.5}As$ barriers was grown. In the growth process, lateral migration of Ga atoms from the flat quantum well areas towards the sidewall occurs. This results in an increase of quantum well width up to 13 nm at the sidewall, thus creating a quasi-one-dimensional confinement of carriers over a lateral width of about 50 nm. Such a single quantum wire (QWR) was investigated in the NSOM experiments. The low-temperature far-field photoluminescence spectrum of this sample [9, 10] is characterized by two energetically well separated emission peaks at 1.540 and 1.605 eV. The 8.5 meV broad peak at 1.54 eV is assigned to the QWR emission and that at 1.605 eV to emission from the embedding QW.

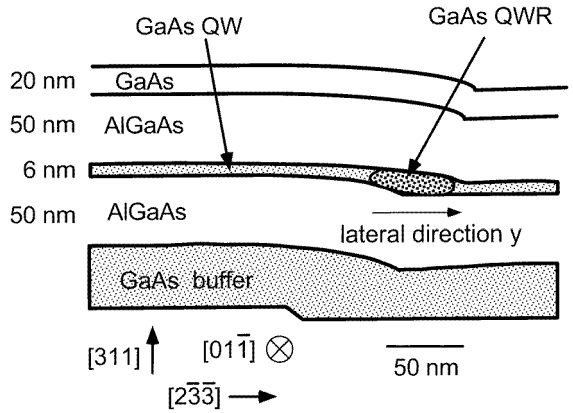

Figure 1. Schematic of the quantum wire structure. The quasi-one-dimensional confinement is due to the lateral thickness variation of the GaAs quantum well.

The NSOM measurements were performed with a near-field microscope designed for operation in the wide temperature range from 10 to 300 K [11]. The sample is mounted on the cold finger of a helium cryostat which is placed in a vacuum chamber. High spatial resolution is achieved by transmitting excitation light through an aperture of about 150 nm diameter at the end of a metal-coated fibre probe. The transmission efficiency of these tips is on the order of 10^{-4}. The distance between the fibre probe and the surface of the sample is held at about 10 nm by a shear-force distance stabilization with the help of a quartz tuning fork on which the fibre tip is mounted [11, 12].

In the experiments reported in sections 3 and 4, the sample is excited through the fibre probe either by continuous-wave HeNe or Ti:sapphire lasers or by femtosecond pulses from a mode-locked Ti:sapphire oscillator. The excitation power on the sample was between 10 and 100 nW, corresponding to very low carrier densities between 10^4 and 10^5 cm^{-1}. The luminescence from the sample was collected with a conventional far-field microscope objective. The luminescence was dispersed in a 0.22 m double monochromator (spectral resolution 1.2 nm) and detected

with a silicon avalanche diode, either in steady state or time resolved with a resolution of 250 ps. Both photoluminescence (PL) and photoluminescence excitation (PLE) spectra of the quantum wire sample were recorded.

3. Mapping of the lateral quantum wire potential

In this section, we present results of spatially resolved PLE experiments under steady-state conditions which provide direct insight into the lateral confinement potential of the quantum wire. In a first series of measurements, the quantum wire luminescence was recorded as a function of the excitation energy and the position of the excitation tip on the sample. Data for a sample temperature of 10 K were reported in [13] and give evidence of the quasi-one-dimensional subband structure in our sample. The spatial resolution in this measurement was 250 nm, mainly determined by the geometry of the sample with the quantum wire 70 nm below the sample surface. In figure 2, spatially resolved PLE data for a sample temperature of 77 K are displayed. The intensity of quantum wire luminescence at 1.533 eV, the luminescence maximum, is plotted as a function of the excitation energy and the lateral distance y of the excitation tip from the quantum wire position at $y = 0$. For photon energies below 1.60 eV, quantum wire emission occurs exclusively for resonant quantum wire excitation at the wire position ($y = 0$), resulting in the spatially narrow structure in figure 2. Strong QWR luminescence is also detected for excitation of the embedding QW at energies higher than 1.6 eV and at distances y of up to several μm away from the QWR location, both on the mesa top ($y > 0$) and bottom ($y < 0$). This is evident from the bright areas of figure 2 at lateral separations y of up to several micrometres. At each excitation position, the PLE spectrum at energies above 1.6 eV shows a pronounced peak and, at higher energies, a spectrally continuous emission intensity. Both the energetic position of the low-energy peak and the spectral shape of the PLE spectrum for $y \neq 0$ change strongly with excitation position. This is highlighted in figure 3 where cross sections through the data in figure 2 are shown. The position of the lowest PLE maximum (indicated by the solid line) shifts towards higher photon energies as the excitation tip approaches the quantum wire location. At each excitation position the PLE spectra recorded for QW excitation reflect the *local* QW absorption spectrum. The dominant features of these spectra are the excitonic QW absorption peak and the continuum absorption at higher energies. The spectra at each excitation position were analysed in detail on the basis of the Elliott expression for the absorption spectrum of a quasi-two-dimensional semiconductor, as has been discussed elsewhere [14]. The main information that is extracted from this analysis is the energetic position of the local excitonic QW absorption peak and the local bandgap energy as a function of excitation position. In figure 4, the position of the excitonic QW absorption peak derived from such a treatment is plotted as a function of lateral distance y. This peak in the spectra shifts by about 14 meV to higher energies as one moves from a distance of $y = 5.5$ μm to the location of the QWR. On the mesa bottom ($y < 0$), this shift is even more pronounced with PLE maxima at 1.610 eV for $y = -3.5$ μm and 1.628 eV for $y = -0.4$ μm.

The complete lateral confinement potential of the quantum-well-embedded quantum wire structure is now derived. Two different spatial regions are distinguished. In the region $|y| > 100$ nm the potential can directly be obtained from figure 4. In the central 100 nm around $y = 0$ the lateral potential is given by the QWR PLE spectrum at 10 K [13], and independently by the lateral thickness variation of the quantum well layer that was determined from cross-sectional TEM images [9]. In the inset of figure 4, this lateral potential is shown as a function of y for the whole interval between -2 and +2 μm. The standard ratio of 2:1 for the conduction to valence band offset energy in quasi-two-dimensional $GaAs/Al_{0.5}Ga_{0.5}As$ structures was used in this analysis. The lateral variation of bandgap energy found in the near-

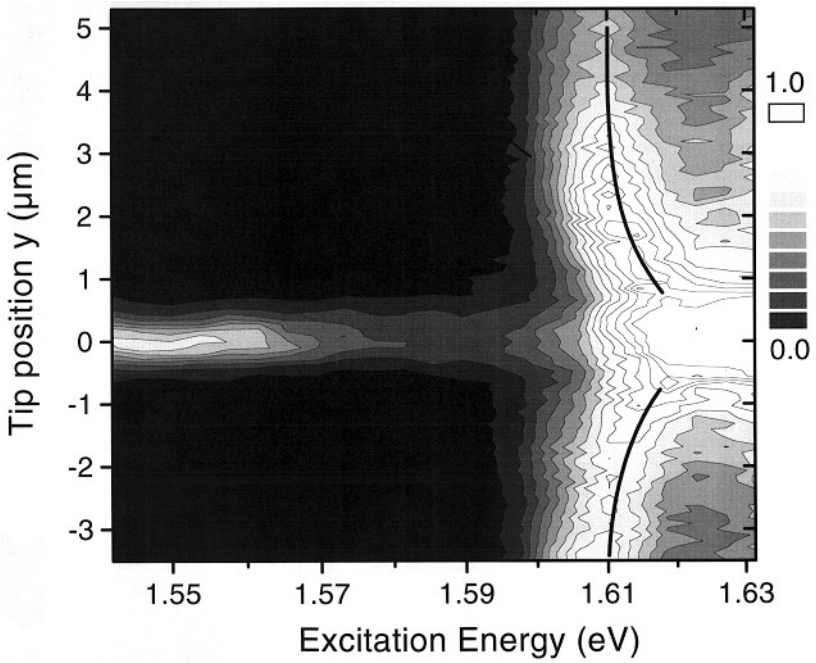

Figure 2. Near-field PLE spectrum of the quantum wire structure at a sample temperature of 77 K. The intensity of quantum wire luminescence at a photon energy of 1.533 eV is plotted as a function of the lateral separation between the exciting fibre tip and the quantum wire at $y = 0$ (ordinate) and as a function of the excitation energy (abscissa). At small photon energies, emission is found only for excitation at the quantum wire location. At photon energies higher than 1.61 eV, excitation of the surrounding quantum well results in quantum wire emission.

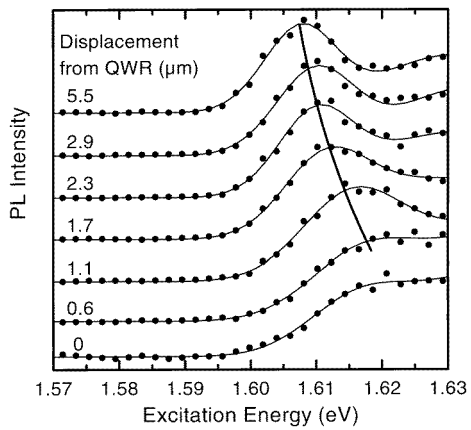

Figure 3. Cross sections through figure 2 for different separations y between excitation tip and quantum wire. The peak is due to excitonic enhancement of the quantum well absorption and displays a blue-shift with decreasing separation from the wire.

field measurements results in the broad shallow barriers adjacent to the quantum wire (see figure 1). The quasi-one-dimensional subband structure and the interband transition energies

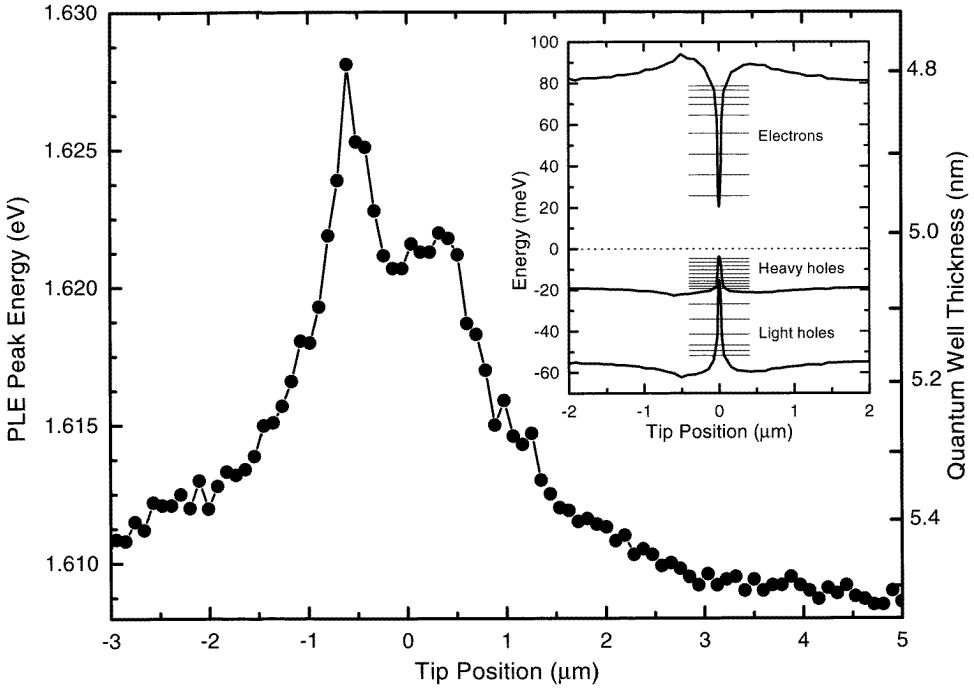

Figure 4. Lateral bandgap profile as derived from the data in figures 2 and 3. The energy of the excitonic peak in the PLE spectra is plotted versus lateral separation from the quantum wire. The lateral variation of the peak position is caused by a change of the average quantum well thickness in the range close to the quantum wire. Inset: quantum wire confinement potential and calculated energies of the quasi-one-dimensional subbands.

of the QWR are now calculated within the adiabatic approximation for solving the Schrödinger equation, neglecting Coulomb correlation effects. The 1D subband energies and interband transition energies displayed in the inset of figure 4 (lines) are in reasonable agreement with the low-temperature PLE spectrum reported in [13].

There are essentially two mechanisms from which the broad barriers in the vicinity of the quantum wire could originate, (i) a local variation of quantum well thickness due to the growth mechanism which involves lateral transport of Ga atoms, or (ii) strain induced by growing the quantum wire on a prestructured mesa-like substrate. We recorded a series of low-temperature (10 K) excitation spectra of quantum well luminescence to clarify this issue. In figure 5, spatially resolved PLE spectra at a detection energy of 1.598 eV (near the maximum of the QW emission peak) are presented. The relatively strong intensity fluctuations in those spectra are due to the localization of excitons at low temperature which translates into local variations of the luminescence transition energies. For photon energies between 1.605 eV and 1.63 eV, one finds a continuous blue-shift of the onset of quantum well absorption with decreasing separation from the quantum wire, in agreement with the data of figure 4. The central dark area around $y = 0$ corresponds to the region between the two shallow barriers where carriers are trapped very efficiently into the quantum wire and—consequently—do not contribute to quantum well luminescence. Figure 6 gives a cross section through figure 5 for different separations from the quantum wire position. Both the heavy and light hole peak in the quantum well excitation spectra are resolved. The two peaks show a continuous blue-

shift with decreasing distance from the quantum wire whereas the energy separation of the two peaks, i.e. the heavy–light hole splitting, remains essentially unchanged. The absolute value of this splitting of about 35 meV is in good agreement with theoretical estimates for an unstrained 6 nm wide GaAs quantum well. We conclude from this agreement and from the constant heavy–light hole splitting that strain plays a minor role for the observed blue-shift of the excitonic peaks. Instead, the shift is related to a local thinning of the quantum well in the range of the shallow barriers. This thinning is a consequence of the Ga atom migration towards the sidewall in the growth process and is determined by the specific MBE growth parameters, e.g., the substrate temperature. The right-hand ordinate scale in figure 4 gives the quantum well thickness corresponding to the PLE peak positions found in the experiment. The asymmetry in the bandgap profile on mesa top ($y > 0$) and bottom ($y < 0$) is most likely related to the wet chemical etching procedure that is used to pattern the mesa structure and the resulting changes of the mobility of Ga atoms during growth.

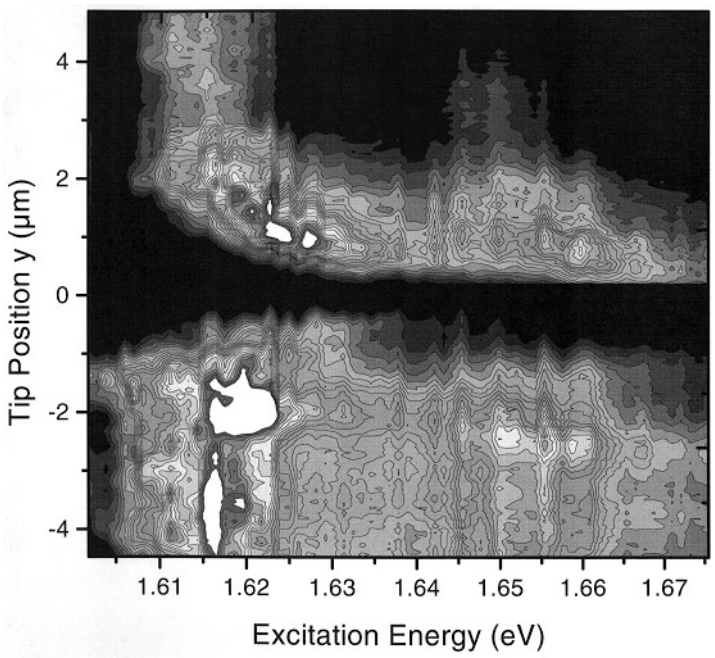

Figure 5. Near-field PLE spectrum of the quantum well for a lattice temperature of 10 K (detection energy 1.598 eV). The data taken for photon energies between 1.605 eV and 1.63 eV reveal the continuous blue-shift of the onset of quantum well absorption with decreasing separation from the quantum wire, in agreement with the data of figure 2.

It should be noted that the energetic positions of the different quasi-one-dimensional subbands are mainly determined by the central part of the confinement potential whereas the outer barriers play a minor role. Such barriers, however, are important for carrier transport from the surrounding quantum well into the quantum wire as will be discussed in the next section.

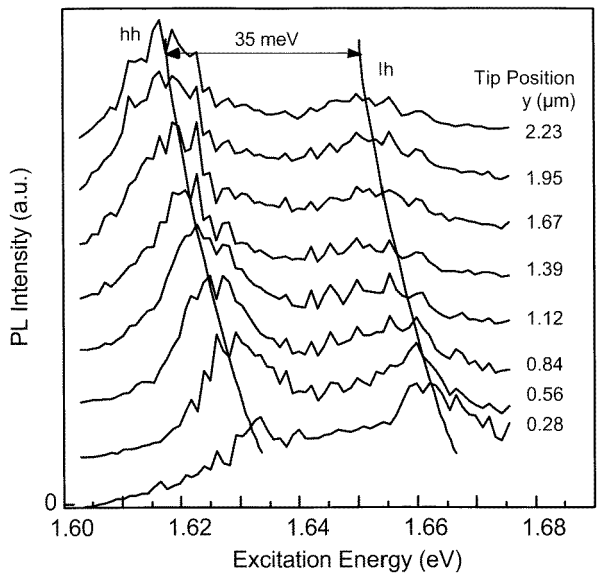

Figure 6. Cross sections through figure 5 for different separations y between excitation tip and quantum wire. Both the heavy and the light hole excitonic peaks of the quantum well PLE spectrum show a blue-shift when approaching the quantum wire. In contrast, the energy separation of the heavy and light hole peaks is nearly the same for all y values.

4. Real-space transfer of excitons

Experimental techniques combining high spatial and temporal resolution allow detailed studies of real-space transfer and trapping of excitons and/or electron–hole pairs in the quantum wire structure. In our experiments, resonant femtosecond excitation through the near-field probe creates a highly localized distribution of quantum well excitons at a well defined separation y from the location of the quantum wire [11]. Real-space transfer of these excitons and trapping into the quantum wire give rise to quantum wire luminescence. A time-resolved measurement of luminescence intensity reveals the rise time of emission which is determined by the dynamics of real-space transfer and trapping, and the decay of emission due to recombination.

At a sample temperature of 10 K, the barriers in the vicinity of the quantum wire suppress a transfer of carriers from the quantum well into the quantum wire very efficiently. As a result, quantum wire emission is found only for excitation tip positions between the two barriers, as is also evident from the spatially resolved quantum wire PLE spectrum at 10 K [9] and other steady state PL measurements [14]. In figure 7, we present data for a higher sample temperature of 100 K. At this temperature and the low excitation densities in our experiments, transport is dominated by the real-space transfer of excitons [15]. The time evolution of quantum wire luminescence is plotted for different values of y, the lateral distance between the excitation spot and the quantum wire location. The solid line at early times gives the instrumental response function demonstrating a time resolution of 250 ps. For excitation on the quantum wire ($y = 0$), the luminescence intensity rises within the time resolution and decays monoexponentially (inset: logarithmic plot of the transients) with a recombination time of 1.5 ns. This result demonstrates that trapping of carriers from the high lying states populated by optical excitation at 1.614 eV, to the bottom of the quantum wire from where the

emission at a photon energy of 1.54 eV originates, occurs much faster than our time resolution. Trapping is connected with the emission of longitudinal optical phonons and characterized by time constants on the order of 1 ps [16].

With increasing separation of the excitation spot from the quantum wire location, one observes a continuous increase of the rise time of quantum wire luminescence, as is evident from the transients for $y = 0.4$, 1.0 and 2.0 μm (figure 7). This delay reflects the finite travelling time of excitons from the area of excitation to the quantum wire, i.e. the dynamics of real-space transfer. The decrease of the overall luminescence intensity for increasing y is due to the fact that a bigger fraction of quantum well excitons undergoes recombination already in the quantum well, i.e. on its way to the quantum wire. The data in figure 7 were recorded with excitation on the mesa top. On the mesa bottom ($y < 0$), a similar luminescence kinetics is found; however, the maximum luminescence intensities are smaller. This behaviour is caused by the somewhat higher barrier on the mesa bottom which has to be passed by the excitons and leads to a lower fraction of trapped carriers.

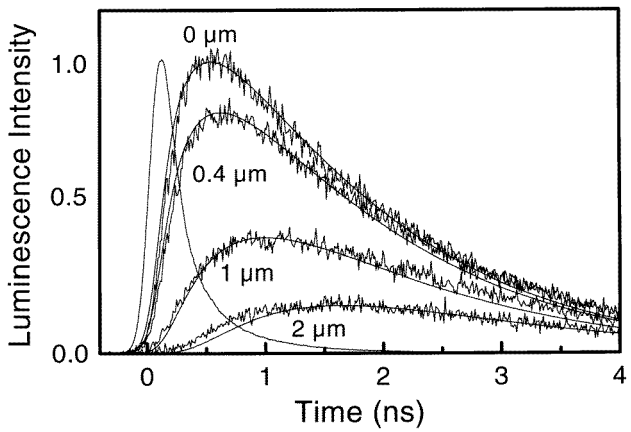

Figure 7. Time evolution of the quantum wire luminescence for different separations y between excitation tip and quantum wire (sample temperature 100 K). The luminescence intensity (linear scale) at 1.54 eV is plotted as a function of time and shows an increasingly delayed rise with increasing y (excitation energy 1.614 eV). This reflects the transport time of excitons from the excitation spot to the quantum wire.

Exciton transport is described by a two-dimensional particle current density $\boldsymbol{j}(\boldsymbol{r}, t) = \boldsymbol{j}_{diff}(\boldsymbol{r}, t) + \boldsymbol{j}_{drift}(\boldsymbol{r}, t)$ with a diffusion term $\boldsymbol{j}_{diff}(\boldsymbol{r}, t) = -D_{ex}\boldsymbol{\nabla} n(\boldsymbol{r}, t)$ induced by the gradient of the exciton concentration $n(\boldsymbol{r}, t)(\boldsymbol{r} = (x, y)$, D_{ex}: exciton diffusion coefficient) and a drift term $\boldsymbol{j}_{drift}(\boldsymbol{r}, t) = -\mu_{ex} n(\boldsymbol{r}, t)\boldsymbol{\nabla} U(\boldsymbol{r})$ induced by the action of the local band gap gradient $\boldsymbol{\nabla} U(\boldsymbol{r})$ on the centre of mass motion of the exciton (μ_{ex}: equivalent charged particle mobility of the exciton) [17]. Under the conditions of our experiment, μ_{ex} is linked to the diffusion coefficient D_{ex} by the Einstein relation $\mu_{ex} = eD_{ex}/kT$ (e: electron charge, k: Boltzmann constant). The evolution of the exciton concentration $n(\boldsymbol{r}, t)$ in space and time is described by the two-dimensional continuity equation, including a generation, a diffusion, a drift and a recombination term:

$$\frac{\partial n(\boldsymbol{r}, t)}{\partial t} = g(\boldsymbol{r}, \boldsymbol{r}_0, t) + D_{ex}\Delta n(\boldsymbol{r}, t) + \mu_{ex} n(\boldsymbol{r}, t)\Delta U(\boldsymbol{r}) + \mu_{ex}\boldsymbol{\nabla} n(\boldsymbol{r}, t)\boldsymbol{\nabla} U(\boldsymbol{r}) - n(\boldsymbol{r}, t)/\tau(\boldsymbol{r}). \quad (1)$$

Here, the spatial variation of the band gap $U(\boldsymbol{r})$ along the lateral y-direction, perpendicular to

the wire axis, is directly taken from the confinement potential in figure 4. The exciton lifetime $\tau(\boldsymbol{r})$ has a value of 1.5 ns for the quantum wire and 1.35 ns for the quantum well. For the generation term $g(\boldsymbol{r}, t)$, we use a Gaussian shape in time (FWHM of 1 ps) and space (FWHM of 300 nm) centred at $\boldsymbol{r} = (0, y)$. The intensity of the time-resolved QWR luminescence is proportional to $I(t) = \int \mathrm{d}x \int \mathrm{d}y\, \partial n(\boldsymbol{r}, t)/\partial t$, where the integration is performed over the length of the QWR along the x-axis and over the width of the QWR region along the y-axis. For comparison with experiment, $I(t)$ is convoluted with the temporal response function of the photodetector (solid line in figure 7). The solid lines in figure 7 represent the result of such simulations for different tip positions y. For an exciton diffusion coefficient $D_{ex} = 13\,\mathrm{cm}^2\,\mathrm{s}^{-1}$, there is very good agreement of the calculations and the experimental results both for $y < 0$ and $y > 0$. This diffusion coefficient corresponds to an excitonic mobility $\mu_{ex} = 1500\,\mathrm{cm}^2\,\mathrm{V}^{-1}\,\mathrm{s}^{-1}$ in the quantum well, given mainly by hole mobility of and limited in this temperature range by LO phonon scattering.

The model calculation correctly describes the influence of the lateral band gap variation $U(\boldsymbol{r})$ on the exciton transport. In the region outside the barriers, $U(\boldsymbol{r})$ exerts a force on the excitonic centre of mass motion that opposes the diffusive real space transfer towards the quantum wire. This is manifested in the experimental data as (i) a significantly weaker QWR luminescence for mesa bottom ($y < -0.4\ \mu$m) than mesa top ($y > 0.4\ \mu$m) excitation due to the higher barrier on the mesa bottom, and (ii) a slight shift of the temporal position of the maximum of the quantum wire emission t_{max} to shorter delay times on the mesa top. Both on the mesa top and bottom, the calculated t_{max} are in good agreement with the measured values (see figure 4), indicating that the exciton diffusion constants are similar on both sides of the quantum wire. In contrast, in the region inside the barriers, $|y| < 0.4\ \mu$m, the bandgap variation $U(\boldsymbol{r})$ accelerates the exciton transport towards the wire, explaining directly the fast rise of the PL decay curve within the time resolution of the present experiment.

5. Outlook: femtosecond near-field spectroscopy

A temporal resolution in the femtosecond regime is required for studying the trapping and the subsequent redistribution of carriers in the quantum wire. For combining femtosecond techniques with near-field spectroscopy, the following issues have to be addressed:

- Femtosecond pulses propagating through the fibre probe experience a substantial broadening in time because of the group velocity dispersion in the fibre. In addition to this linear effect, self-phase modulation of the pulses due to the third-order nonlinearity of the fibre material, in general quartz, occurs at high intensities and leads to an additional broadening of the pulse spectrum.
- The transmission of the sub-wavelength aperture at the end of the fibre probe has very small values of about 10^{-4}. As a result, collection of light from the sample, e.g. luminescence, through the fibre probe is connected with very high losses and femtosecond detection schemes like time-resolved luminescence up-conversion are very difficult to implement. For pump–probe experiments with pulses transmitted through the aperture, the pump intensity is limited and the weak probe light has to be discriminated from the luminescence of the sample and other optical background.

Based on those considerations, we designed an experimental setup for femtosecond two-colour pump–probe measurements in a near-field microscope. A schematic of this experiment is shown in figure 8. Pump and probe pulses are derived from a modelocked Ti:sapphire oscillator providing 50 fs pulses tunable in the wavelength range from 810 to 870 nm. This laser works at a repetition rate of 80 MHz and gives an average power of up to several hundreds

of milliwatts. The laser output is split into a pump and a probe beam each of which travels through a prism setup for spectral selection and precompensation of group velocity dispersion in the subsequent optical components. The pump beam is mechanically chopped at a frequency f_1 and focused onto the sample by a far-field $f = 8$ cm graded index lens, resulting in a spot size on the sample of about 30 μm. The average pumping powers are up to about 10 milliwatts. The probe beam has an average power of a few milliwatts in order to limit self-phase modulation in the fibre which has a typical length of 50 cm. The probe beam is chopped at a frequency f_2, fed into the fibre probe and transmitted onto the sample through the sub-wavelength aperture at the end of the fibre probe. The time delay between pump and probe is adjusted with the delay stage in the pump beam. After interaction with the sample, the transmitted or the reflected probe light is collected through standard microscope lenses and detected by a photodiode in conjunction with a lock-in amplifier. For suppression of background signals, the lock-in amplifier detects an electrical signal at the sum frequency $f_1 + f_2$.

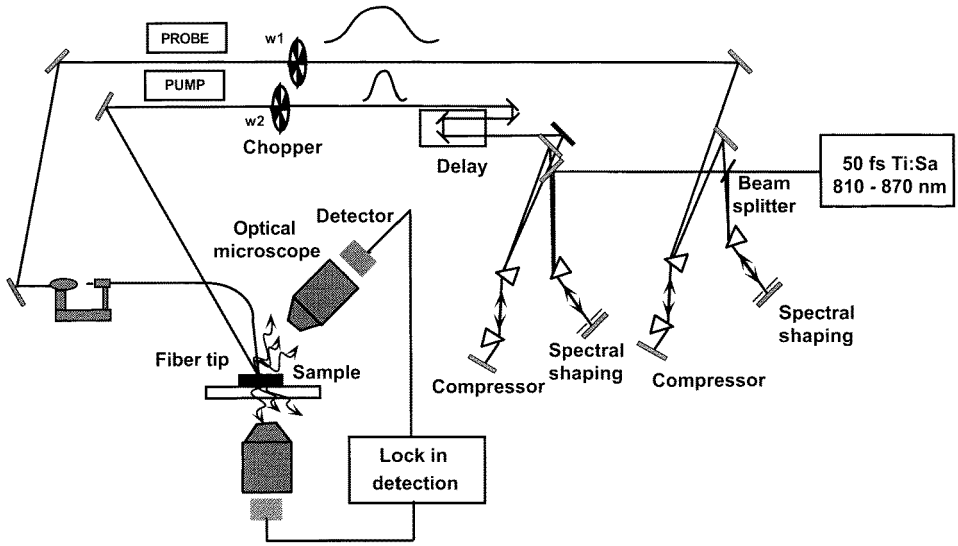

Figure 8. Schematic of the experimental setup for femtosecond near-field spectroscopy. Pump and probe pulses are derived from a mode-locked Ti:sapphire laser using two independent arrangements for spectral shaping and compression. The pump excites a large area of the sample whereas the probe is fed into a near-field probe, allowing for a spatially resolved detection of ultrafast transmission or reflection changes. The nonlinear changes of transmission or reflection are measured with the help of a lock-in technique.

First pump–probe measurements were performed with the quantum wire sample at room temperature. In figure 9, we present the result of a reflectivity measurement performed with the near-field probe located above the quantum well area of the sample. The 50 fs excitation pulse at a centre wavelength of 815 nm (bandwidth 30 nm) creates approximately 10^{11} electron–hole pairs per cm^2. The resulting change of reflectivity is probed at 815 nm, slightly below the band edge of the quantum well (probe bandwidth 9 nm). In figure 9, the change of reflectivity is plotted as a function of time delay between pump and probe pulses. The creation of electron–hole pairs results in a steplike increase of reflectivity which is due to the transient decrease of the refractive index at this wavelength position [18]. The decrease of refractive index depends on the specific probe wavelength, resulting in a change of the signal amplitude with wavelength (inset of figure 9). The carrier concentration in the quantum well rises instantaneously with

the density of absorbed photons, i.e. follows in time the integral over the excitation pulse, and decays by recombination on a much longer time scale. The signal in figure 9 represents the convolution of this steplike response with the envelope of the probe pulses. An analysis of the rising part of the transient gives a time resolution better than 200 fs for this measurement. This demonstrates that the broadening of the probe pulse in the fibre probe is fully precompensated in the prism compressor/selector. The spatial resolution determined independently has a value of about 300 nm. The high sensitivity of the experiment allows the detection of reflectivity changes as small as 10^{-4}.

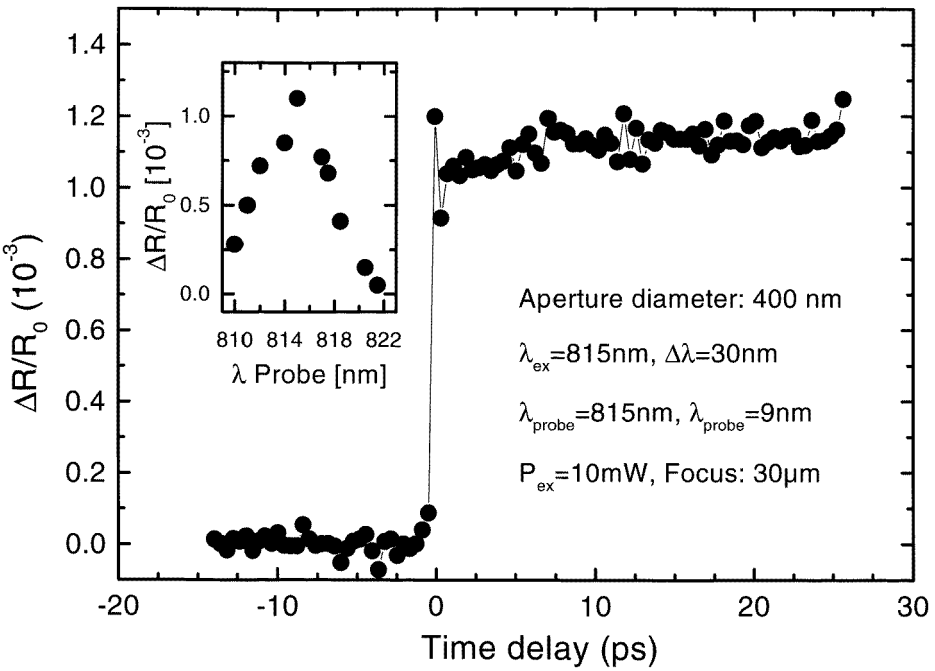

Figure 9. Reflectivity change of the quantum wire sample measured with the setup of figure 8. The change of reflectivity $\Delta R/R_0 = (R - R_0)/R_0$ probed in the quantum well area is plotted as a function of the delay time between the pump pulse at 815 nm (bandwidth 30 nm) and the probe pulse at the same wavelength (bandwidth 9 nm; R, R_0: reflectivity of the sample with and without excitation). Inset: amplitude of the signal for different probe wavelengths (sample temperature 300 K).

6. Conclusions

In conclusion, single quantum well embedded GaAs quantum wires were studied by spatially and temporally resolved near-field spectroscopy in a wide temperature range. The lateral confinement potential of the quantum wire and the quasi-one-dimensional subband structure were determined in steady-state photoluminescence and photoluminescence excitation measurements. We demonstrated the existence of broad shallow barriers in the vicinity of the quantum wire which originate from a thinning of the embedding quantum well in the growth process. Such barriers suppress carrier transport from the quantum well into the quantum wire at low temperatures around 10 K. Exciton transport and trapping was studied in picosecond luminescence at elevated temperatures. An analysis of those results on the basis

of a drift-diffusion model gives an exciton mobility of 1500 $cm^2\ V^{-1}\ s^{-1}$ at 100 K. Finally, we presented first femtosecond pump–probe experiments with a near-field microscope. This highly sensitive technique allows the investigation of ultrafast nonequilibrium carrier dynamics on nanometre length scales. Experiments on carrier trapping and redistribution in a single quantum wire are at present under way.

Acknowledgments

We thank R Nötzel, M Ramsteiner and K Ploog for the quantum wire sample studied in our experiments. Financial support by the Deutsche Forschungsgemeinschaft (Sonderforschungsbereich 296) and by the European Union (TMR network 'Ultrafast') is gratefully acknowledged. VE thanks the European Union for support as a TMR–Marie Curie fellow.

References

[1] Tsuchiya M, Gaines J M, Yan R H, Simes R J, Holtz P O, Coldren L A and Petroff P M 1989 *Phys. Rev. Lett.* **62** 466
[2] Kapon E, Hwang D M and Bhat R W 1989 *Phys. Rev. Lett.* **63** 430
[3] Goni A R, Pfeiffer L N, West K W, Pinczuk A, Baranger H U and Störmer H L 1992 *Appl. Phys. Lett.* **61** 1956
[4] Pohl D W, Denk W and Lanz M 1984 *Appl. Phys. Lett.* **44** 651
[5] Betzig E, Trautman J K, Harris T D, Weiner J S and Kostelak R L 1991 *Science* **251** 1468
[6] Xie X S and Dunn R C 1994 *Science* **265** 361
[7] Ambrose W P, Goodwin P M, Martin J C and Keller A R 1994 *Science* **265** 364
[8] Richter A, Süptitz M, Heinrich D, Lienau Ch, Elsaesser T, Ramsteiner M, Nötzel R and Ploog K H 1998 *Appl. Phys. Lett.* **73** 2176
[9] Nötzel R, Ramsteiner M, Menniger J, Trampert A, Schönherr H P, Däweritz L and Ploog K H 1996 *Japan. J. Appl. Phys.* **35** L297
[10] Richter A, Süptitz M, Lienau Ch, Elsaesser T, Ramsteiner M, Nötzel R and Ploog K H 1997 *Surf. Interface Anal.* **25** 583
[11] Behme G, Richter A, Süptitz M and Lienau C 1997 *Rev. Sci. Instrum.* **68** 3458
[12] Karrai K and Grober R D 1995 *Appl. Phys. Lett.* **66** 1842
[13] Richter A, Behme G, Süptitz M, Lienau Ch, Elsaesser T, Ramsteiner M, Nötzel R and Ploog K H 1997 *Phys. Rev. Lett.* **79** 2145
[14] Lienau Ch, Richter A, Süptitz M, Heinrich D, Elsaesser T, Ramsteiner M, Nötzel R and Ploog K H 1998 *Phys. Rev.* B **58** 2045
[15] Hillmer H, Forchel A and Tu C W 1992 *Phys. Rev.* B **45** 1240
[16] Ryan J F, Maciel A C, Kiener C, Rota L, Turner K, Freyland J M, Marti U, Martin D, Morier-Gemoud F and Reinhart F K 1996 *Phys. Rev.* B **53** R4225
[17] Tamor M A and Wolfe J P 1980 *Phys. Rev. Lett.* **44** 1703
[18] Lee Y H *et al* 1986 *Phys. Rev. Lett.* **57** 2446